Kinetic Study of the Gas-Phase Reaction of $Ca(^1S_0)$ with O_2 from 296 to 623 K

Mark L. Campbell*,†

Chemistry Department, United States Naval Academy, Annapolis, Maryland 21402

John M. C. Plane

School of Environmental Sciences, University of East Anglia, Norwich, NR4 7TJ, United Kingdom

Received: October 17, 2000; In Final Form: December 15, 2000

The reactivity of gas-phase ground-state calcium atoms with O_2 is reported from 296 to 623 K. Calcium atoms were produced by the photodissociation of $Ca(FOD)_2$ [where FOD represents the 6,6,7,7,8,8,8-heptafluoro-2,2-dimethyl-3,5-octanedionate ion] and detected by laser-induced fluorescence. Calcium recombines with O_2 to form CaO_2 in a reaction that exhibits a positive temperature dependence and is significantly in the falloff region even at pressures as low as 10 Torr. Ab initio quantum calculations are used to show that the reaction most likely proceeds on a triplet surface, where the Ca atom inserts into the O−O bond to form a triplet dioxide ($^3B_2$) with a very low frequency bending mode. The surprisingly large rate coefficient at elevated temperatures is explained by the correspondingly high density of rovibrational states, and the positive temperature dependence by a small barrier in the entrance channel at the crossing point between the covalent and ionic diabats. RRKM theory, fitted to the experimental data, predicts the following expression for the rate coefficient from 140 to 1000 K and 10^{-5} to 10^3 Torr: $\log(k_{rec,0}/cm^6\ molecule^{-2}\ s^{-1}) = -57.10 + 19.70 \log T - 3.410(\log T)^2$, $k_{rec,\infty} = 1.36 \times 10^{-10} \exp(-1020/T)\ cm^3\ molecule^{-1}\ s^{-1}$, and $F_c = 0.67$.

Introduction

The recombination reaction

$$Ca + O_2 + N_2 \rightarrow CaO_2 + N_2 \qquad (1)$$

is of both fundamental and applied interest. Uncommon for a recombination reaction, the rate coefficient has a pronounced positive temperature dependence between 200 and 1000 K,[1,2] although increasingly this appears to be the case for recombination reactions of metal atoms that have closed s shells.[3] The two earlier experimental studies of reaction 1, which employed the pulsed laser photolysis/laser induced fluorescence method[1] and the fast flow tube technique,[2] are in reasonably good agreement at temperatures between 300 and 400 K. However, the flow tube study indicated that the rate coefficient should continue to increase above 1000 K, whereas the flash photolysis study revealed a marked slowing of the rate coefficient at 1100 K. Compounding this experimental uncertainty is the problem that ab initio studies of CaO_2[1,4] find that the Ca−O_2 bond energy is only about 200 kJ mol^{-1}, which would appear not to be large enough to permit rapid recombination of Ca and O_2 at elevated temperatures.

Reaction 1 is of practical interest in understanding the chemistry of calcium in the Earth's upper mesosphere. Calcium, along with several other metals, ablates from the approximately 100 tons of interplanetary dust that enters the atmosphere daily.[5] These metals exist as thin layers of metal atoms that occur globally at an altitude of about 90 km. Atomic Ca, along with Na, Fe, and K, can be observed from the ground by the lidar (or laser radar) technique. Lidar has revealed the enormous depletion of Ca by a factor of more than 120 with respect to Na, compared to their relative abundances in chondritic meteorites.[6] This very puzzling observation could be explained either by Ca ablating less efficiently from meteoroids,[7] or through differences in the chemistries that control the formation of the metal atom layers. CaO_2 is a potential sink for Ca, and can be formed either directly by reaction 1, or via the reaction sequence $Ca + O_3 \rightarrow CaO + O_2$ followed by $CaO + O_3 \rightarrow CaO_2 + O_2$.[6] Another unusual feature of the Ca layer is that during summer, when the upper mesosphere is very cold, the abundance of Ca below 90 km actually increases, in direct contrast to Na. This could be related to the slower formation of CaO_2 through reaction 1.

Here we report an experimental determination of the third-order rate constants of reaction 1 to help resolve the inconsistencies in the previous two studies. In addition, quantum calculations on CaO_2 are described, and the experimental rate constants are fitted by application of RRKM theory.

Experimental Section

The experimental arrangement has been described in detail elsewhere and will be described only briefly here.[8] Pseudo-first-order kinetic experiments ($[Ca] \ll [O_2]$) were carried out in an apparatus with slowly flowing gas using a laser photolysis/laser induced fluorescence (LIF) technique. Laser photolysis of a metal precursor, $[Ca(FOD)_2$, where FOD represents the 6,6,7,7,8,8,8-heptafluoro-2,2-dimethyl-3,5-octanedionate ion] produced the gas-phase calcium metal atoms and laser induced fluorescence was used to probe their temporal behavior. The reaction chamber is a stainless steel reducing four-way cross with attached sidearms and a sapphire window for optical viewing. The reaction chamber is enclosed within a convection oven (Blue M, Model 206F, $T_{max} = 623$ K) with holes drilled

† Henry Dreyfus Teacher−Scholar.

10.1021/jp003808e CCC: $20.00
Published on Web 03/08/2001

to allow for the exiting sidearms and the telescoping of the LIF signal to the PMT.

Calcium atoms were produced by the 248 nm photodissociation of $Ca(FOD)_2$ with the focused output of an excimer laser (Lambda Physics Lextra 200). The focusing lens ($f = 564$ mm) was placed approximately one focal length from the reaction zone. Typical laser pulse energies were approximately 200 mJ. Calcium atoms were detected via LIF using an excimer-pumped dye laser (Lambda Physics Lextra 50/ScanMate 2E) tuned to 422.67 nm. The fluorescence was detected at 90° to the counterpropagated laser beams with a three-lens telescope imaged through an iris. A narrow-band interference filter centered at 420 nm was used to isolate the LIF. A photomultiplier tube (Hamamatsu R375) was used in collecting the LIF which was subsequently sent to a gated boxcar sampling module (Stanford Research Systems SR250), and the digitized output was stored and analyzed by a computer. Real time viewing of the photolysis prompt emission and LIF signal were accomplished using a LeCroy Model 9360 digital oscilloscope.

Due to the low vapor pressure at room temperature, the calcium precursor required gentle heating in order to get enough precursor into the gas phase. The precursor vapor was entrained in a flow of N_2 buffer gas. The diluted precursor, N_2 buffer, and O_2 flowed through calibrated mass flow meters and flow controllers (MKS Types 1459C and 0258C) prior to admission to the reaction chamber. Each sidearm window was purged with a slow flow of buffer gas to prevent deposition of calcium atoms and other photoproducts. Total flows varied between 200 and 3300 sccm (sccm = standard cubic centimeters per minute); however, most experiments used a flow of approximately 600 sccm. Pressures were measured with MKS Baratron manometers, and chamber temperatures were measured with a thermocouple.

The delay time between the photolysis pulse and the dye-laser pulse was varied by a digital delay generator (Stanford Research Systems DG535) controlled by a computer interfaced through a Stanford Research Systems SR245 computer interface. The trigger source for these experiments was scattered pump laser light incident upon a fast photodiode. LIF decay traces typically consisted of 200 data points, and each point averaged four laser shots.

Materials. $Ca(FOD)_2$ (Strem), O_2 (MG Industries, 99.8%), and N_2 (Potomac Airgas, Inc., 99.998%) were used as received.

Data Analysis and Results

The decay rates of gas-phase calcium atoms as a function of oxygen pressure were investigated as a function of temperature and total pressure. Under pseudo-first-order conditions in which no production processes occur after the initial photolysis event, the decrease in the [Ca] with time following the photolysis laser pulse is given by

$$-\mathrm{d[Ca]}/\mathrm{d}t = (k_{\mathrm{rec}}[\mathrm{O_2}] + k_{\mathrm{d}})[\mathrm{Ca}] = (1/\tau)[\mathrm{Ca}] \qquad (2)$$

where k_{rec} is the observed second-order rate constant due to O_2 at a fixed buffer gas pressure, k_{d} represents the depletion rate constant due to the reaction of the calcium with precursor molecules and fragments and diffusion out of the detection zone, and τ is the observed time constant for calcium depletion in the presence of a given $[O_2]$, precursor, and buffer gas pressure. The LIF signal is proportional to the calcium metal number density, [Ca]. Thus, for a simple pseudo-first-order system in which production of excited states is insignificant, the LIF signal

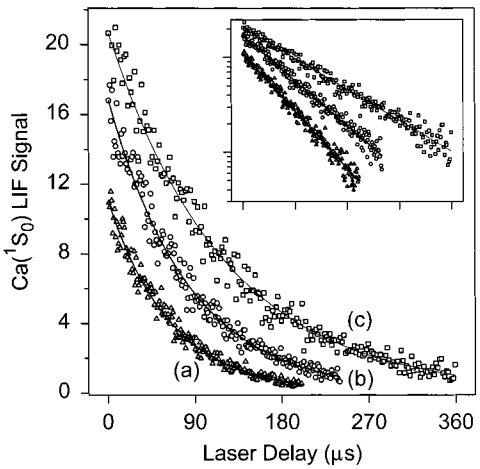

Figure 1. Typical $Ca(^1S_0)$ decay curves with added O_2 at 296 K and $P_{\mathrm{total}} = 5.0$ Torr: (a) $P(O_2) = 744$ mTorr, $\tau = 64.3$ μs; (b) $P(O_2) = 557$ mTorr, $\tau = 82.8$ μs; (c) $P(O_2) = 371$ mTorr; $\tau = 120$ μs. The solid lines through the data are exponential fits. The inset is a natural logarithm plot of the data.

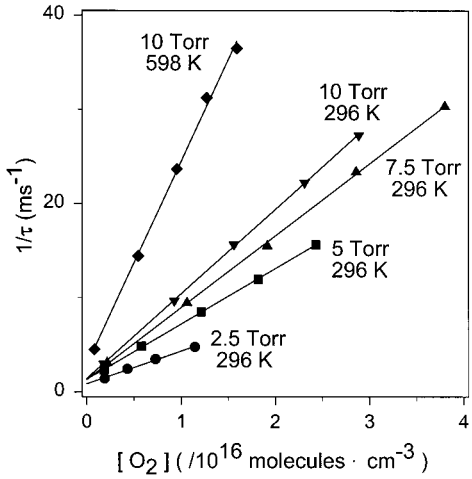

Figure 2. Typical plots for determining k_{rec} for $Ca(^1S_0) + O_2$ illustrating the third-order behavior of this reaction. The solid line for each set of data is a linear regression fit from which k_{rec} is obtained.

of the ground state at a time t after photolysis is

$$[\mathrm{Ca}](t) \propto \mathrm{LIF}(t) = \mathrm{LIF}_0 \exp(-t/\tau) \qquad (3)$$

where LIF_0 is the initial LIF signal immediately following the photolysis laser pulse. LIF decays that exhibit single-exponential behavior were fitted using a least-squares procedure to determine τ.

Typical plots of exponential decays are shown in Figure 1. Once the reaction time constant has been determined for a series of oxygen number densities, the slope of a plot of $1/\tau$ vs $[O_2]$ yields the observed second-order rate constant, k_{rec}. Figure 2 illustrates examples of these types of plots. The rate constants for the reaction of Ca with O_2 were found to be pressure dependent. Figure 2 illustrates the pressure and temperature dependence of the second-order rate constants for this reaction. The relative uncertainty (i.e., the reproducibility) of the second-order rate constants is estimated at ±20% based on repeated measurements of rate constants under identical temperature and total pressure conditions. The absolute uncertainties are conservatively estimated to be ±30% and are based on the sum of the statistical scatter in the data, uncertainty in the flowmeter and flow controller readings (5%) and the total pressure reading

TABLE 1: Second-Order Rate Constants k_{rec} (10^{-12} molecule^{-1} cm^3 s^{-1}) for the Reaction $Ca + O_2 + N_2 \rightarrow CaO_2 + N_2$ as a Function of Temperature and Pressure

	pressure (Torr)			
T (K)	2.5	5.0	7.5	10.0
296	0.35	0.59	0.76	0.90
348	0.48	0.78	1.0	1.3
373	0.55	0.80	1.2	1.5
398	0.59	0.93	1.2	1.5
423	0.60	0.96	1.3	1.6
448	0.61	1.0	1.4	1.7
473	0.60	1.0	1.5	1.7
498	0.64	1.1	1.5	1.9
523	0.64	1.1	1.5	1.9
548	0.61	1.1	1.5	1.8
573	0.66	1.1	1.6	2.0
598	0.65	1.2	1.7	2.2
623	0.61	1.2	1.6	2.0

(1%), uncertainties due to incomplete gas mixing, and uncertainties due to incomplete relaxation of the excited electronic states to the ground state.

Measured rate constants for $Ca(^1S_0)$ with O_2 as a function of temperature at 2.5, 5.0, 7.5, and 10.0 Torr are listed in Table 1. In addition, room-temperature measurements were measured at 20.0, 50.0, 75.0, and 100 Torr; $k_{rec} = 1.4 \times 10^{-12}$, 2.2×10^{-12}, 2.5×10^{-12}, and 2.7×10^{-12} cm^3 molecule^{-1} s^{-1}, respectively.

Discussion

To understand these results and to extrapolate the rate coefficient outside the experimental pressure and temperature range, we now describe a set of quantum calculations on CaO_2 followed by the application of RRKM theory to reaction 1. The singlet and triplet forms of CaO_2 were examined using the hybrid density functional/Hartree−Fock B3LYP method from within the Gaussian 98 suite of programs.[9] Geometries were first optimized using the reasonably large 6-311+G(2d,p) triple-ζ basis set, which has both polarization and diffuse functions added to the atoms.[10] For the linear O−Ca−O forms of these molecules, the initial self consistent field (SCF) wave function was found to be unstable and was reoptimized. The resulting geometries, dipole moments, rotational constants, and vibrational frequencies are listed in Table 2, together with the Ca−O_2 bond energies. Note that these were calculated with respect to neutral Ca and O_2 rather than Ca^+ and O_2^- (in which case they would be smaller by 8 kJ mol^{-1} after correcting with the experimental ionization energy of Ca and electron affinity of O_2). At the level of theory employed here the expected uncertainty in the calculated D_0(Ca−O_2) is ±14 kJ mol^{-1}.[10]

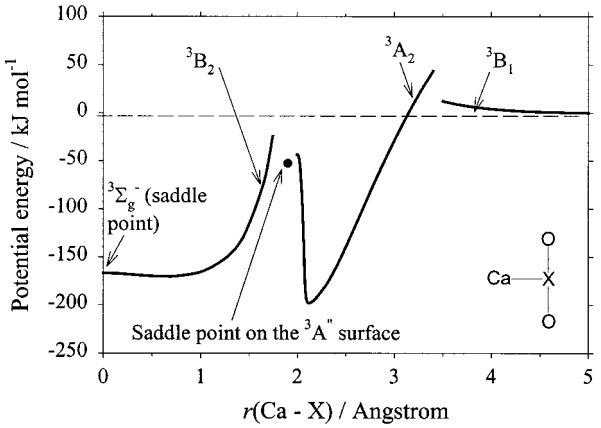

Figure 3. Potential energy curves for the reaction between Ca and O_2 under C_{2v} symmetry. The curves were calculated at the B3LYP/6-311+G(2d,p) level of theory as a function of r(Ca−X) (X is defined in the figure), while constraining the r(Ca−O) distance as appropriate (see text).

Table 2 shows that very satisfactory agreement was achieved with a previous high-level ab initio study by Bauschlicher et al.,[4] as well as a more recent and extensive set of calculations reported by Andrews et al.[12] The most stable form of CaO_2 is the $^1A_1$ state. This state is produced when Ca vapor and O_2 are co-condensed in a low-temperature matrix. Table 2 shows that the theoretical vibrational frequencies are in very good accord with the matrix measurements of Andrews and co-workers,[11,12] considering that the matrix environment can cause shifts of several tens of cm^{-1} compared with the isolated molecule in the gas phase. Andrews et al.[12] also reported an asymmetric stretch for $CaO_2(^3B_2)$, with which the present theory is in excellent agreement (Table 2).

Unlike the matrix environment, $CaO_2(^1A_1)$ may not be formed in reaction 1 since the reaction will occur, at least initially, on a triplet surface. There is further discussion of this point below. Figure 3 illustrates the triplet potential energy curves for the approach of Ca to O_2 in a C_{2v} configuration. These curves were calculated at the B3LYP/6-311+G(2d,p) level of theory. For the $^3B_1$ and outer branch of the $^3A_2$ curves, r(O−O) was fixed

TABLE 2: Optimized Geometries and Molecular Parameters for the Most Stable Singlet and Triplet Forms of CaO_2, Calculated at the B3LYP/ 6-311+G(2d,p) Level of Theory[a]

species	geometry	dipole moment[b]	rotational constants[c]	vibrational frequencies[d]	$D_0(CaO_2)$[e]
$CaO_2(^1A_1)$	r(CaO) = 1.98 Å,	10.4	27.4, 8.51, 6.49	502 [501 (N_2)[f]],	229 ± 14
C_{2v} symmetry	r(OO) = 1.52 Å;			623 [556 (N_2)[f]],	[226 ± 17,[h]
	∠CaO = 45.1°			806 [742 (N_2),[f] 736 (Ar)[g]]	198−248[f]]
$CaO_2(^3A_2)$	r(CaO) = 2.21 Å,	2.9	35.4, 6.44, 5.45	372, 444, 1191	195 ± 14
C_{2v} symmetry	r(OO) = 1.34 Å;				[188,[h] 184−204[f]]
	∠CaO = 35.2°				
$OCaO(^3\Sigma_g^-)$	r(CaO) = 2.01 Å	0.0	3.91	41*i*, 42, 462, 561	171 ± 14
linear saddle point					
$CaO_2(^3B_2)$	r(CaO) = 2.13 Å;	4.6	62.1, 3.86, 3.64	70, 481, 529	174 ± 14
C_{2v} symmetry	r(OO) = 4.04 Å;			[497 (N_2),[f] 516 (Ar)[g]]	[161−196[f]]
	∠CaO = 143.0°				
$CaO_2(^3A'')$	r(CaO) = 2.03 Å,	7.44	21.3, 7.89, 5.76	1258*i*, 355, 622	56 ± 14
transition state	r(CaO) = 2.14 Å,				
$^3A_2 \leftrightarrow {}^3B_2$	r(OO) = 1.73 Å;				
	∠CaO = 49.0°				

[a] Previous theoretical and experimental estimates are shown in brackets. The molecules are listed in order of decreasing Ca−O_2 bond strength. [b] In debyes (=3.336 × 10^{-30} C m). [c] In GHz. [d] In cm^{-1}. [e] In kJ mol^{-1}. [f] Reference 12, measurement in N_2 matrix. [g] Reference 11, measurement in Ar matrix. [h] Reference 4, ab initio theory.

at 1.21 and 1.34 Å, respectively, and r(Ca−X) varied (X is defined in Figure 3). For the repulsive inner branch of the $^3A_2$ curve, and all of the $^3B_2$ curve, r(Ca−O) was fixed at 2.21 and 2.13 Å, respectively, and the O−Ca−O angle varied. The reaction begins initially on a covalent $^3B_1$ surface. A charge transfer then occurs to produce the most stable triplet form of $CaO_2(^3A_2)$, a classical isosceles triangular superoxide molecule with r(O−O) = 1.34 Å, corresponding to the O_2^- ion. There is then a further minimum where the Ca atom inserts into the O_2 to form a dioxide, the triangular $^3B_2$ state. Note that this state is only slightly more stable than linear $CaO_2(^3\Sigma_g^-)$, which is actually a saddle point (Figure 3 and Table 2). As shown in Figure 9 of Nien et al.,[1] the situation for the dioxides reverses for MgO_2, where there are no d orbitals on the metal atom to stabilize the bent $^3B_2$ form. As expected, the Mulliken charge on the Ca increases from +0.57 in the superoxide to +1.2 in the dioxides.

If the reaction between Ca and O_2 occurred in a strictly C_{2v} configuration, then there would have to be a nonadiabatic transition from the $^3B_1$ onto the $^3A_2$ surface, and from the $^3A_2$ onto the $^3B_2$ surface, giving rise to significant electronic barriers (Figure 3). However, in C_s symmetry, where the Ca attack is well away from side-on to the O_2, the reaction can proceed on a $^3A''$ surface all the way from Ca + O_2 through the superoxide to the dioxide. B3LYP/6-311+G(2d,p) calculations show that the barrier to the initial charge transfer disappears, and the barrier between the superoxide and dioxide is 56 kJ mol^{-1} (including zero-point energies) *below* the energy of the reactants Ca + O_2 (Table 2). Thus, the Ca atom can insert unhindered into the O_2 bond, *except* for near side-on attack.

We now apply RRKM theory to reaction 1, using the master equation (ME) formalism developed by De Avillez Pereira et al.[13] We have recently described the application of this formalism to recombination reactions of metallic species,[14] so only a brief description is given here. The reaction is considered to proceed via the mechanism

$$\mathrm{Ca} + \mathrm{O_2} \rightarrow \mathrm{CaO_2}^* \qquad (1.1)$$

$$\mathrm{CaO_2}^* \rightarrow \mathrm{Ca} + \mathrm{O_2} \qquad (-1.1)$$

$$\mathrm{CaO_2}^* + \mathrm{N_2} \rightarrow \mathrm{CaO_2} + \mathrm{N_2} \qquad (1.2)$$

The energy of the adduct CaO_2 was first divided into a contiguous set of grains (width 30 cm^{-1}), each containing a bundle of rovibrational states of average energy, E_i. Each grain was then assigned a set of microcanonical rate coefficients for dissociation, $k^{-1}(E_i)$. The ME describes the evolution with time of the grain populations

$$\frac{\mathrm{d}}{\mathrm{d}t}\rho_i(t) = \omega\sum_j P_{ij}\rho_j(t) - \omega\rho_i(t) - k^{-1}(E_i)\,\rho_i(t) + R_i \qquad \text{(I)}$$

where R_i is the rate of population of $CaO_2(E_i)$ via reaction 1.1, ω is the frequency of collisions between CaO_2* and N_2, and P_{ij} is the probability of transfer of CaO_2 from grain j to grain i on collision with N_2. The individual P_{ij} were estimated using the exponential down model,[15] with the average energy for downward transitions ($i < j$), $\langle\Delta E\rangle_{\mathrm{down}}$, an adjustable parameter between 150 and 400 cm^{-1} for N_2. For upward transitions where $j > i$, P_{ij} was calculated by detailed balance. To use the ME to simulate irreversible stabilization of CaO_2 via reaction 1.2, an absorbing boundary was set 24 kJ mol^{-1} below the energy of the reactants so that collisional energization from the boundary to the threshold was highly improbable. The rate of population

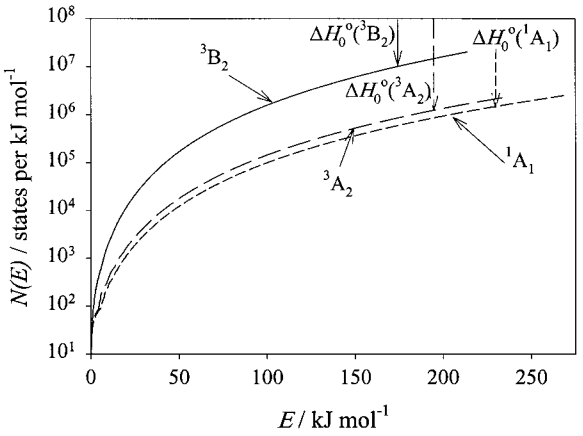

Figure 4. Plot of the density of rovibrational states $N(E)$ as a function of internal excitation energy E, for the three strongly bound electronic states of CaO_2. The arrows indicate the position of the bond energy of each state, which represents a lower limit to the critical energy for recombination.

of grain i, R_i, is given by detailed balance between reactions 1.1 and −1.1:

$$R_i = k_{\mathrm{rec},\infty}[\mathrm{Ca}][\mathrm{O_2}]\eta_i \qquad \text{(II)}$$

where $k_{\mathrm{rec},\infty}$ is the limiting high-pressure association rate coefficient (reaction 1.1) and

$$\eta_i = \frac{k_i^{-1}}{\sum_i k_i^{-1} f_i} \qquad \text{(III)}$$

where f_i is the equilibrium Boltzmann distribution of $CaO_2(E_i)$.

The microcanonical rate coefficients for dissociation of CaO_2 were determined using inverse Laplace transformation,[13] which links $k^{-1}(E_i)$ directly to $k_{\mathrm{rec},\infty}$. In the present case, $k_{\mathrm{rec},\infty}$ was expressed in the Arrhenius form $A^\infty \exp(-E^\infty/RT)$. The microcanonical rate coefficient for dissociation is then given by

$$k^{-1}(E_i) = \frac{A^\infty(2\pi\mu)^{3/2}}{N(E_i)\,\Gamma(1.5)h^3}\int_0^{E_i - E^\infty - \Delta H_0°} N_{\mathrm{p}}(x)[(E_i - E^\infty - \Delta H_0°) - x]^{0.5}\,\mathrm{d}x \qquad \text{(IV)}$$

where the density of states of $CaO_2(^3B_2)$ at energy E_i, $N(E_i)$, was calculated using a combination of the Beyer−Swinehart algorithm for the vibrational modes (without making a correction for anharmonicity) and a classical densities of states treatment for the rotational modes; $N_{\mathrm{p}}(E_i)$ is the convoluted density of states of Ca and O_2; $\Delta H_0{}^o$ is the Ca−O_2 bond energy; and μ is the reduced mass of Ca and O_2. Note that in the case of the $^3B_2$ state, the lowest vibrational mode is only 70 cm^{-1}, corresponding to a flapping motion across the $^3\Sigma_g^-$ saddle point. Since this motion is likely to be highly anharmonic,[15] $N(E_i)$ was multiplied by a factor of 1.72.[16]

The ME was expressed in matrix form[13] and then solved to yield k^{calc}, the bimolecular recombination rate constant at a specified pressure and temperature. Calculations were performed for recombination to form the $^1A_1$, $^3A_2$ and $^3B_2$ states of CaO_2. However, only the $^3B_2$ state has a sufficiently high density of rovibrational states at the critical energy ($E_0 \approx \Delta H_0° + E^\infty$) for k^{calc} to approach the experimental measurements above 400 K, let alone account for the observed positive temperature dependence. Figure 4 illustrates the energy dependence of $N(E)$,

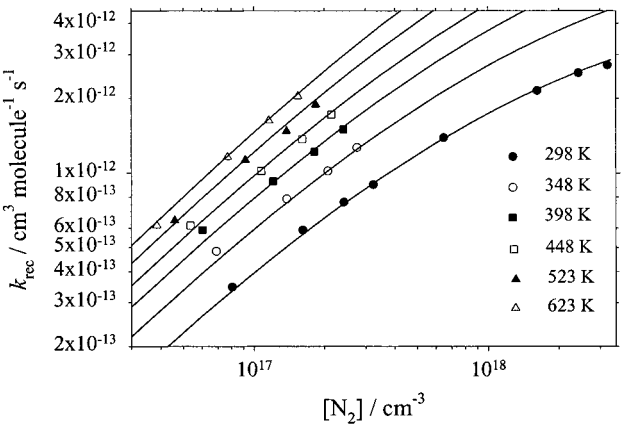

Figure 5. Pressure dependence of the reaction of Ca($^1S_0$) + O_2 in N_2 buffer, at a selection of temperatures. The points are experimental data, and the lines are RRKM theory from a global fit.

showing that, even though the $^3B_2$ state is less strongly bound, the density of states when $E_0 = \Delta H_0^o$ is at least an order of magnitude higher compared with the $^3A^2$ and $^1A^1$ states. Thus, we conclude that recombination occurs primarily through the $^3B_2$ dioxide.

To fit k^{calc} to the experimental data in Table 1, six adjustable parameters were allowed. These were the Arrhenius parameters A^∞ and E^∞ which define $k_{rec,\infty}$; the parameters σ and ϵ/k describing the intermolecular potential between CaO_2 and N_2, from which ω was calculated; the average energy for downward transitions, $\langle\Delta E\rangle_{down}$; and α, which defines the (small) T^α dependence of $\langle\Delta E\rangle_{down}$. These parameters were varied in a simple grid search to minimize χ^2, defined as

$$\chi^2 = \sum_i^N \left(\frac{k_{rec,i} - k^{calc,i}}{\sigma_i} \right)^2 \qquad \text{(V)}$$

i.e., the sum over N experimental points of the squared difference between the measured $k_{rec,i}$ (with uncertainty σ_i) and the modeled value $k^{calc,i}$. The best fit parameters are $A^\infty = 1.36 \times 10^{-10}$ cm^3 molecule^{-1} s^{-1}, $E^\infty = 8.47$ kJ mol^{-1}, $\sigma = 4.55$ Å, $\epsilon/k = 450$ K, $\langle\Delta E\rangle_{down} = 350$ cm^{-1}, and $\alpha = 1.74$. The largest deviation between k^{calc} and k_{rec} was 11.6%, with an average deviation of 4.2%. This very satisfactory fit of RRKM theory to the experimental data over a range of pressure and temperature is illustrated in Figure 5.

The value of E^∞ implies a small barrier of about 6.7 kJ mol^{-1} (cf. the value of 5.5 kJ mol^{-1} obtained in a previous fit to kinetic data on reaction 1, and the significantly larger barrier of 26 kJ mol^{-1} for the analogous reaction between Mg and O_2[1]). This barrier most likely occurs in the reaction entrance channel where the covalent reactants exchange an electron to form the superoxide, and is a spatial average between the large barrier for near-C_{2v} collisions and barrierless transitions at other geometries (except for near collinear). This barrier is more likely to control the kinetics of reaction 1 than the barrier between the superoxide and dioxide, for two reasons. First, the barrier on the $^3A''$ surface between the $^3A_2$ and $^3B_2$ states is substantially below the energy of the reactants (Figure 3) and has near-C_{2v} geometry (Table 2), so the impact of the nonadiabatic transition required in a strictly C_{2v} collision is likely to be minor. Second, the matrix isolation study of Andrews et al.[12] did not observe the $^3A_2$ state, whereas $^3B_2$ formed readily in the low-temperature environment. It should be noted that CaO_2($^1A_1$) was also observed, particularly in the N_2 matrix. However, the matrix may well have assisted with the change in spin required to form this state. In the gas phase, recombination to form $^1A_1$, even assuming a unit probability for the nonadiabatic triplet−singlet transition, is not fast enough to account for the measured values of k_1. A final point here is that the fitted value of A^∞ is a factor of 3−4 below the collision frequency between Ca and O_2. This may reflect in part the steric constraints for side-on collisions, but A^∞ is also likely to incorporate the probability of adiabatic charge transfer occurring on the $^3A''$ surface where the covalent and ionic diabats cross.

To provide a simple expression for extrapolating k^{calc} over a large range of temperature (140−1000 K) and pressure (10^{-5} to 10^3 Torr), we have expressed the T-dependence of $k_{rec,0}$ as a second-order polynomial in log T, and then fitted the theoretical results to the Lindemann expression modified by a broadening factor F_c:

$$k^{calc} = \frac{k_{rec,0}[M]}{1 + \dfrac{k_{rec,0}[M]}{k_{rec,\infty}}} F_c^{\,K}$$

where

$$K = \frac{1}{\left\{1 + \left(\log\left(\dfrac{k_{rec,0}[M]}{k_{rec,\infty}}\right)\right)^2\right\}} \qquad \text{(VI)}$$

$\log(k_{rec,0}/\text{cm}^6\ \text{molecule}^{-2}\ \text{s}^{-1}) = -57.10 + 19.70 \log T - 3.410(\log T)^2$, $k_{rec,\infty} = 1.36 \times 10^{-10} \exp(-1020/T)$ cm^3 molecule^{-1} s^{-1}, and $F_c = 0.67$.

The uncertainties involved in using RRKM theory to extrapolate k^{calc} outside the experimental range of temperature and pressure was estimated using the following procedure. The individual uncertainty of each of the six fitted parameters was assigned to be that which caused χ^2 in eq V to double. A set of six parameters was then chosen by Monte Carlo sampling of each parameter, assuming a uniformly random distribution within each parameter's range of uncertainty. k^{calc} was then calculated at 298, 473, and 623 K over the experimental pressure range. If k^{calc} fell within the experimental uncertainty (±30%) of k_{rec} , then this set of parameters was used to extrapolate k^{calc} to mesospheric and flame conditions. This criterion allows for the fact that the fitted parameters are not all independent of each other. The procedure was repeated until 200 successful Monte Carlo selections and extrapolations had been performed. The uncertainty in the extrapolated k^{calc} is then given by 2 standard deviations about the mean of the 200 estimates of k^{calc}. Under mesospheric conditions, where the pressure was chosen to be 3×10^{-3} Torr corresponding to an altitude of about 85 km, the results are: k(140 K) = (5.1 ± 2.8) × 10^{-17}, k(190 K) = (2.0 ± 0.9) × 10^{-16}, and k(240 K) = (4.1 ± 1.5) × 10^{-16} cm^3 molecule^{-1} s^{-1}. Under flame conditions, k(2000 K, 760 Torr) = (3.0 ± 0.6) × 10^{-11} cm^3 molecule^{-1} s^{-1}. Of course, these uncertainties do not allow for the possible roles of the $^3A_2$ and $^1A_1$ states of CaO_2 in reaction 1, but these are expected to be minor for the reasons discussed earlier.

Figure 6 is a three-dimensional mesh plot of k^{calc} versus pressure and temperature, illustrating once again the excellent agreement with the experimental points from the present study. Note the unusual morphology of the surface caused by the falloff in k^{calc} as a function of pressure *and* temperature. The experimental points below 650 K from the earlier study of Nien et al.[1] are also shown for comparison. In general, the agreement is quite satisfactory: the present results are on average 23% lower, with the difference ranging from −95% to +21%. The

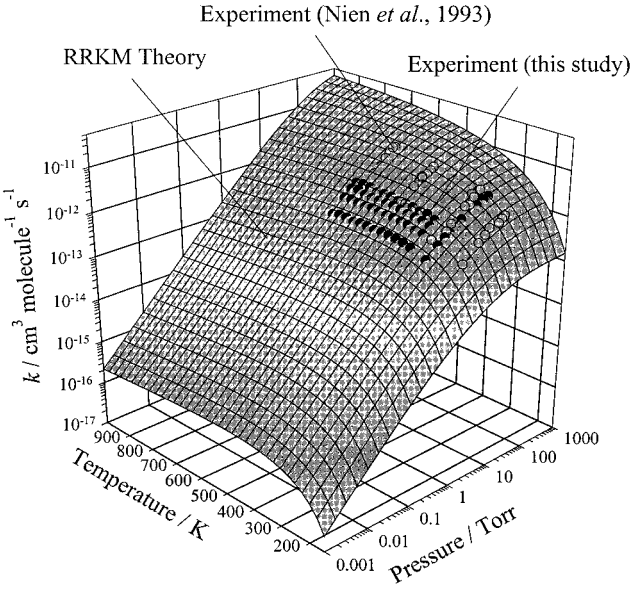

Figure 6. Mesh plot of the recombination rate coefficient for $Ca(^1S_0) + O_2$ in N_2, calculated from RRKM theory as a function of temperature and pressure. Experimental points from the present study (dark circles) and ref 1 (white circles) are also shown.

generally higher results in the earlier study were most likely caused by reactions involving O_2 with the photolytic precursors, as reported by Nien et al.,[1] and so a more detailed comparison with the RRKM fit to the present data is not warranted. However, Nien et al.[1] also reported high-temperature measurements of $k(1107\ \text{K}) = 2.1 \times 10^{-13}$ and 3.6×10^{-13} cm^3 molecule^{-1} s^{-1} at 19.2 and 36.3 Torr, respectively. Inspection of Figure 6 shows that in comparison with the RRKM extrapolation, these high-temperature measurements are too low by about an order of magnitude. The most likely explanation for this was the role of atomic I produced from CaI_2, the photolytic precursor of Ca atoms used in the earlier study.[1] This precursor was employed because organometallic calcium compounds decompose at considerably lower temperatures. It was noted by Nien et al.[1] that O_2 reacted with CaI_2 on the hot reactor walls above 400 K to generate I_2, which was then observed to react rapidly with Ca in the gas phase. In contrast, above 1000 K I_2 is overwhelmingly dissociated to atomic I, and so I_2 was assumed not to be a significant contaminant in the high-temperature measurements.

However, it now appears that atomic I could have played the following role. As shown in Table 2, the triplet forms of CaO_2 have bond energies below 200 kJ mol^{-1}. Indeed, at 1107 K and 19−36 Torr, the present RRKM calculations indicate that the thermal dissociation rate coefficient of CaO_2 should be large, ranging from 600 to 1040 s^{-1}. Thus, in a flash photolysis experiment the initial decay of Ca in the presence of O_2 at elevated temperatures should be rapid, but then cease as a steady state between recombination and dissociation is achieved. However, in the experiments of Nien et al.[1] this was not observed, most probably because atomic I reacted with CaO_2 to yield $CaI + O_2$, a reaction that is exothermic by about 100 kJ mol^{-1}. This reaction would then have controlled the disappearance of Ca, at a rate slower than the initial formation of CaO_2 due to reaction 1. The rate would have been proportional to the atomic I concentration and the steady-state concentration of CaO_2, both a function of the O_2 concentration in the reactor. The I atom concentration would also have been proportional to the residence time of the O_2 gas mixture in the hot reactor. Since the total pressure was changed by altering this residence time, the loss of Ca would also have appeared to be pressure-dependent, leading to the erroneous measurement.

Conclusions

The present study appears to resolve the discrepancy between the two earlier studies[1,2] of the recombination reaction between Ca and O_2. Furthermore, the use of quantum calculations and RRKM theory show that the surprisingly large rate coefficient at elevated temperatures can be explained very satisfactorily by the high density of rovibrational states of the triplet dioxide form of CaO_2, and the positive temperature dependence by a small barrier in the entrance channel at the crossing point between the covalent and ionic diabats.

Acknowledgment. This research was supported by a Cottrell College Science Award of Research Corporation and Award GR3/11754 from the Natural Environment Research Council of the U.K.

References and Notes

(1) Nien, C.-F.; Rajasekhar, B.; Plane, J. M. C. *J. Phys. Chem.* **1993**, *97*, 6449.
(2) Vinckier, C.; Remeysen, J. *J. Phys. Chem.* **1994**, *98*, 10535.
(3) Plane, J. M. C. In *Gas-Phase Metal Reactions*; Fontijn, A., Ed.; Elsevier: Amsterdam, 1992.
(4) Bauschlicher, C. W., Jr.; Partridge, H.; Sodupe, M.; Langhoff, S. R. *J. Phys. Chem.* **1992**, *96*, 9259.
(5) Plane, J. M.C. *Int. Rev. Phys. Chem.* **1991,** *10*, 55.
(6) Gerding, M.; Alpers, M.; von Zahn, U.; Rollason, R. J.; Plane, J. M. C. *J. Geophys. Res.* **2000**, *105*, 27131.
(7) von Zahn, U.; Gerding, M.; Höffner, J.; McNeil, W. J.; Murad, E. *Meteoritics Planet. Sci.* **1999**, *34*, 1017.
(8) Campbell, M. L.; McClean, R. E. *J. Chem. Soc., Faraday Trans.* **1995**, *91*, 3787.
(9) Frisch, M. J.; Trucks, G. W.; Schlegel, H. B.; Scuseria, G. E.; Robb, M. A.; Cheeseman, J. R.; Zakrzewski, V. G.; Montgomery, J. A., Jr.; Stratmann, R. E.; Burant, J. C.; Dapprich, S.; Millam, J. M.; Daniels, A. D.; Kudin, K. N.; Strain, M. C.; Farkas, O.; Tomasi, J.; Barone, V.; Cossi, M.; Cammi, R.; Mennucci, B.; Pomelli, C.; Adamo, C.; Clifford, S.; Ochterski, J.; Petersson, G. A.; Ayala, P. Y.; Cui, Q.; Morokuma, K.; Malick, D. K.; Rabuck, A. D.; Raghavachari, K.; Foresman, J. B.; Cioslowski, J.; Ortiz, J. V.; Baboul, A. G.; Stefanov, B. B.; Liu, G.; Liashenko, A.; Piskorz, P.; Komaromi, I.; Gomperts, R.; Martin, R. L.; Fox, D. J.; Keith, T.; Al-Laham, M. A.; Peng, C. Y.; Nanayakkara, A.; Gonzalez, C.; Challacombe, M.; Gill, P. M. W.; Johnson, B.; Chen, W.; Wong, M. W.; Andres, J. L.; Gonzalez, C.; Head-Gordon, M.; Replogle, E. S.; Pople, J. A. *Gaussian 98*, Revision A.7; Gaussian, Inc.: Pittsburgh, PA, 1998.
(10) Foresman, J. B.; Frisch, A. *Exploring chemistry with electronic structure methods*; Gaussian, Inc.: Pittsburgh, PA, 1996.
(11) Andrews, L.; Yustein, J. T.; Thompson, C. A.; Hunt, R. D. *J. Phys. Chem.* **1994**, *98*, 6514.
(12) Andrews, L.; Chertihin, G. V.; Thompson, C. A.; Dillon, J.; Byrne, S.; Bauschlicher, C. W., Jr. *J. Phys. Chem.* **1996**, *100*, 10088.
(13) De Avillez Pereira, R.; Baulch, D. L.; Pilling, M. J.; Robertson, S. H.; Zeng, G. *J. Phys. Chem.* **1997**, *101*, 9681.
(14) Rollason, R. J.; Plane, J. M. C. *Phys. Chem. Chem. Phys.* **2000**, *2*, 2335.
(15) Gilbert, R. G.; Smith, S. C. *Theory of Unimolecular and Recombination Reactions*; Blackwell: Oxford, 1990.
(16) Troe, J. *J. Chem. Phys.* **1979**, *66*, 4758.